Fabrication of Transparent ITO/GTO Bilayer Thin Films using a Facing Target DC Magnetron Sputtering

Imran bin Sutan Chairul

2023

ABSTRACT

Due to the scarcity of Indium (In) in the future, efforts have been made to fabricate In-free semiconductors such as Ga-Sn-O (GTO) thin films via chemical vapour deposition, RF magnetron sputtering, and DC magnetron sputtering. However, an amorphous GTO fabricated by using DC magnetron sputtering is focused on a specific Ga:Sn ratio, and this opens avenues for further research using other Ga:Sn ratios. Hence, this study fabricated transparent diodes by layering a GTO thin film onto an In_2O_3:Sn (ITO) thin film using a facing targeted DC magnetron co-sputtering method. Ga:Sn ratio was adjusted by varying the current applied to the targets and the number of Ga_2O_3 pellets. Following that, the composition, phase, and optical transmittance of the GTO thin films were characterized. The current–voltage (I–V) characteristics of the fabricated ITO/GTO bilayer diode thin films were also determined. Results show that when a GTO film containing approximately 25 mol% Ga was deposited on the surface of the conductive ITO film at room temperature, a diode bilayer film was obtained. The bilayer film exhibited rectification characteristics of approximately 0 and 3.8 µA/V when negative and positive voltages were applied, respectively. However, the rectification characteristics increased up to 68.3 µA/V in the positive voltage region after annealing at 200 °C.

ACKNOWLEDGMENTS

TABLE OF CONTENTS

LIST OF TABLES

LIST OF FIGURES

CHAPTER 1

INTRODUCTION

1.1   Background of the study

Liquid crystal displays (LCDs), which are widely used in electronic devices, use transparent conductive films and thin film transistors (TFTs) to switch flickering. In recent years, transparent oxide materials based on In–Ga–Zn–O (IGZO) [1] have been increasingly used as semiconductors in TFTs. Amorphous Si has been traditionally used as the primary semiconductor material in such applications. However, Si has certain limitations such as low transparency under visible light and low electrical mobility (0.3–$1.0\,\mathrm{cm^2 \cdot V^{-1} \cdot s^{-1}}$). Therefore, oxide materials with a wide bandgap have been used to overcome these limitations.

1.2   Problem statement

In a previous study, a transparent TFT prototype was fabricated [2], comprising only In_2O_3:Sn (ITO) or In–Ga–Sn–O (GITO) as the electrodes. Although current was successfully controlled by the gate-source voltage, a unidirectional current–voltage behaviour could not be obtained for the transistor. It was hypothesized that ITO (electrode) and GITO (semiconductor layer) both consist of indium oxide-based structures, and the similarity of their electronic structures renders it difficult to create barriers for electron transfer. Therefore, in this study, we fabricated Ga–Sn–O (GTO) semiconductors [3] based on tin oxide instead of GITO semiconductors to obtain rectifying characteristics by depositing GTO film onto ITO film. Moreover, we attempted to control the electrical properties by controlling the number of carriers, which was done by varying the amount of Ga dopant.

1.3   Objectives of the study

The main objectives of this study are as follows:
1.   To fabricate transparent In-Sn-O/Ga-Sn-O (ITO/GTO) bilayer thin films using a facing target DC magnetron sputtering.
2.   To characterize the fabricated GTO thin films.
3.   To evaluate the I–V characteristics of the ITO/GTO bilayer diode thin films.

1.4   Scope of the study

This study is limited within the following scope:

1.   Samples prepared in this study based on the temperature of the glass substrate during deposition of the ITO/GTO bilayer thin films, either room temperature (RT) or 200 °C.

2.   The number of Ga_2O_3 pellets to be simultaneously sputtered with respect to one type of thin film was defined as 'n' and varied from 2 to 3 ($n = 2$ and 3).

1.5   Organization of the thesis

The detailed description for each chapter of this thesis is presented as follows:

Chapter 2 presents a review of the published works pertaining to the research and development of TFTs with different materials of electrodes, semiconductors, insulators, and substrates. The literature is focusing more on silicon-based and metal oxide-based thin film semiconductors used in TFTs and their fabrication methods.

Chapter 3 provides a detailed description of the samples, instruments, and equipment used, preparation methods, and the procedures adopted to fabricate transparent In-Sn-O/Ga-Sn-O (ITO/GTO) bilayer thin films using a facing target DC magnetron sputtering.

In Chapter 4, the results are reported and discussed, beginning with the elemental composition, structure, optical transmittance of the GTO thin films, followed by the I–V characteristics of the ITO/GTO bilayer diode thin films.

Finally, Chapter 5 provides the conclusions drawn based on the findings of this study, as well as recommendations for future work.

CHAPTER 2

LITERATURE REVIEW

2.1   Overview

Nowadays, displays are mostly flat panel displays due to the development of TFTs. TFTs can be categorized into two types: (1) voltage-driven TFTs and (2) current-driven TFTs. Both types apply a switching mechanism that controls the blinking of pixels in a display. Voltage-driven TFTs are used in active matrix liquid crystal displays (AMLCDs) [4] while current-driven TFTs are used in active matrix organic light-emitting diodes (AMOLEDs) [5]. In general, TFTs are fabricated by stacking thin film layers of conductors (gate, source, and drain electrodes), semiconductors, and insulators onto a substrate, where the position of each layer determines the structure of the TFT. There are four types of TFT structures: (1) staggered bottom-gate, (2) coplanar bottom-gate, (3) staggered top-gate, and (4) coplanar top-gate. The conductor, semiconductor, and insulator can be categorized based on their resistivity, ρ ($\Omega \cdot$cm).

The resistivity of a metal conductor is $\sim 10^{-6}$ $\Omega \cdot$cm. On the other hand, the resistivity of a semiconductor is within a range of $\sim 10^{-2}$–10^8 $\Omega \cdot$cm, while the resistivity of an insulator is within a range of $\sim 10^8$–10^{18} $\Omega \cdot$cm. For solid materials, the conductivity is the inverse of resistivity. Conductivity is also proportional to the carrier concentration, n (cm^{-3}), and carrier (hole or electron) mobility, μ (cm$^2 \cdot$V$^{-1} \cdot$s^{-1}), as given by Equation 2.1:

$$\sigma = \frac{1}{\rho} = en\mu \tag{2.1}$$

where e is the elementary charge (1.602×10^{-19} C).

In general, TFTs should have the following characteristics: (1) threshold voltage, V_{th} (V), of ~ 0 V, (2) a small threshold voltage shift, ΔV_{th}, when subjected to the following stresses: operating time, heat, visible light illumination, positive bias, and negative bias, (3) a small sub-threshold swing, S (V$\cdot$dec^{-1}), to ensure fast switching, (4) an appropriate field effect mobility, μ_{FE} (cm$^2 \cdot$V$^{-1} \cdot$s^{-1}), that suits the switching frame rate (Hz) of the display, and (5) a large on-off current ratio, $I_{on}/I_{off} > 10^6$, to optimize the power consumption [6][7][8].

TFTs have been researched and developed with different materials for the electrodes, semiconductors, insulators, and substrates, and this literature review is focused on silicon-based and metal oxide-based thin film semiconductors used in TFTs and their fabrication methods. These topics will be elaborated in the following sub-sections.

2.2 Silicon-based semiconductors

The first functional TFT was reported to use hydrogenated amorphous silicon (a-Si:H) as its semiconductor layer. The a-Si:H was deposited by plasma-enhanced chemical vapour deposition (PECVD). The a-Si:H had the following characteristics: (1) $V_{th} < 3$ V, (2) $S < 0.5$ V·dec^{-1}, (3) $\mu_{eff} < 1$ cm^2·V^{-1}·s^{-1}, (4) $I_{on}/I_{off} > 10^6$ and (5) off-current, $I_{off} < 10^{-12}$ A. These characteristics are considered to be sufficient for AMLCD applications that operate with a pixel switching frame rate of 120 Hz or less. In addition, the amorphous structure of a-Si:H allows fabrication over large areas as well as low cost and high productivity. However, a-Si:H TFTs are not suitable for applications that require a faster switching frame rate (240 Hz) as well as current-driven AMOLED displays because of their low carrier mobility. A large-sized, ultra-definition AMLCD with a frame rate of 240 Hz requires a TFT with a μ_{FE} of more than 5 cm^2·V^{-1}·s^{-1} [7]. In addition, the leakage current of a-Si:H TFT under visible light illumination is quite large since a-Si:H is a photoconductor material [9]. Furthermore, the stability of a-Si:H TFT is a concern since it has large ΔV_{th} over the operating time [10].

Since silicon bonding is covalent, an amorphous state (irregularity in the arrangement of atoms) has made the directionality of its orbit is lost, where the overlapping of carrier paths largely deviates, resulting in a drop in carrier mobility. Owing to the low mobility of a-Si:H TFT, polycrystalline silicon (poly-Si) was developed, where it was fabricated from amorphous silicon (a-Si) by laser annealing. The poly-Si TFT had higher mobility, typically less than 10 cm^2·V^{-1}·s^{-1}, but could be up to 100 cm^2·V^{-1}·s^{-1}, depending on the grain and boundary size [11]. Because of their higher mobility, poly-Si TFTs are suitable for use in current-driven AMOLED displays. However, the fabrication of poly-Si requires a high temperature, which is more costly compared with the fabrication of a-Si:H. The properties of poly-Si are also influenced by exposure to visible light illumination, although to a lesser extent compared with a-Si:H. Furthermore, since poly-Si is crystalline, non-uniformity issues arise due to carrier scattering and trapping of defects at the grain boundaries. This

limits the fabrication of poly-Si TFTs over large areas as well as reproducibility [12]. For this reason, poly-Si TFTs are limited to small-sized AMOLED displays such as mobile phones [7].

2.3 Metal oxide semiconductors

In a quest to search for a potential substitute to silicon-based thin film semiconductors for TFTs, researchers have developed metal oxide semiconductors such as transparent semiconducting oxides (TSOs) and transparent conducting oxides (TCOs). An advantage of metal oxide semiconductors for TFTs is that they can be deposited by conventional sputtering methods. In the sputtering method, metal oxide semiconductors are prepared by using argon, oxygen, or argon/oxygen mixture. In contrast, silicon-based semiconductors are fabricated by using explosive gasses such as silane, phosphine, and diborane. Furthermore, metal oxide semiconductors require low processing temperatures and hence, they are compatible with plastic and flexible substrates. In addition, owing to the large bandgap of metal oxide semiconductors, exposure to visible light illumination will not deteriorate their properties dramatically unlike a-Si:H. Thus, it is not necessary to apply light shields for metal oxide semiconductors used in silicon-based TFTs.

TSOs typically have an intermediate free carrier density, typically within a range of 10^{14}–10^{18} cm^{-3}. In contrast, TCOs have a higher free carrier concentration, normally in the order of 10^{21} cm^{-3}. Both TSOs and TCOs are ionic materials, where the spherical, isotropic ns orbitals of the metallic cations form a conduction band [11][12]. Nowadays, TSO-based TFTs have the following characteristics: (1) V_{th} = ~0 V, (2) S = ~0.2 V·dec^{-1}, (3) $I_{on}/I_{off} >$ 10^7, and (4) μ > 10 cm^2·V^{-1}·s^{-1} [13]. The carrier mobility of metal oxide semiconductors (either crystalline or amorphous) is dependent on the direct overlap between the metal ns orbitals that create a conducting path for free carrier movement. In this regard, it is found that the overlap is maintained in both crystalline and amorphous metal oxide semiconductors since the conducting path is not significantly affected by amorphous structural deformation [7]. Other than maintaining high carrier mobility, which is a typical characteristic of crystalline structures, amorphous oxide semiconductors (AOSs) can be fabricated at room temperature or low processing temperatures (< 500 °C). The formed amorphous phases of metal oxide are also stable when subjected to post-annealing treatment of less than 500 °C,

which is usually applied to modify TFT characteristics. In addition, AOSs exhibit excellent uniformity and surface flatness.

2.3.1 In–Ga–Zn–O

Among TSOs, a single crystalline In–Ga–Zn–O (IGZO) produced at 1400 °C [12] had the following characteristics: (1) V_{th} = ~0 V, (2) S = 0.2–0.3 V·dec^{-1}, and (3) μ_{FE} of 80 cm^2·V^{-1}·s^{-1} [14]. Unlike crystalline IGZO, amorphous In–Ga–Zn–O (a-IGZO) improved the TFT characteristics, where the power consumption was reduced due to its high mobility. The Hall mobility (μ_H) was more than 10 cm^2·V^{-1}·s^{-1} while the saturation mobility (μ_{sat}) of a-IGZO TFT fabricated on polyethylene terephthalate (PET) was within a range of 6–9 cm^2·V^{-1}·s^{-1} [15]. To fabricate an AOS, a-IGZO was deposited onto PET over a large area and at room temperature. Yet, the a-IGZO TFT has a drawback in terms of its stability under negative bias illumination stress (NBIS), where its ΔV_{th} is between −1.4 V and +1.0 V, which is less than 3 V. A ΔV_{th} occurred since a-IGZO contains weak Zn-O bonds [3]. To address the ΔV_{th} issue of a-IGZO, Yamazaki [16] developed c-axis-aligned crystalline (CAAC) IGZO in 2009 where its ΔV_{th} was only 0.5 V (−0.23 V to +0.27 V), which was lower than the ΔV_{th} of a-IGZO.

2.3.2 Ga–Sn–O

Although the IGZO-based TFTs have been developed and widely used for AMLCDs and AMOLEDs, indium (In) is expensive as it is a rare metal [17]. It has been reported that In is commonly recovered from sphalerite or In–Sn–O (ITO) scraps in Japan and Korea [18]. Hence, In-based TSOs are not cost-effective for mass production of TFTs. Ultimately, the demand of displays in the future may not be met due to the scarcity and high price of In. The disadvantages of In have spurred several researchers to develop an In-free TSOs for TFTs. In pursuit of developing In-free TSO, a group of researchers from Ryukoku University developed Ga–Sn–O (GTO), which is a promising alternative to IGZO thin films. The GTO was fabricated by mist chemical vapour deposition (CVD) [19][20] and radio frequency (RF) magnetron sputtering [3][21][22][23].

Fukushima et al. [19] evaluated the relationship between GTO thin films fabricated using mist CVD and the film thickness, transparency, and resistance. The following parameters were varied in their study: (1) Ga:Sn ratio (1:1, 1:2), (2) deposition temperature

(400, 450 °C), (3) carrier gas speed (0.5, 1.0 L·min^{-1}), and deposition time (5–60 min). The results showed that the film thickness increased roughly in proportion to the increase in deposition time and deposition temperature. Furthermore, the transparency of the GTO thin films increased as the deposition temperature decreased. In addition, the resistance of the GTO thin films was found to be dependent on the Ga:Sn ratio but independent of the carrier gas speed. Okamoto et al. [20] evaluated the optical transmittance and sheet resistance of GTO thin films deposited using mist CVD at a Gn:Sn ratio of 1:5. The results showed that the GTO thin films were transparent in the visible light region (wavelength: 380–780 nm), suggesting a wide bandgap. However, the GTO thin films were crystallized. Furthermore, the resistance of the GTO thin films decreased with an increase in the dilution gas, which indicates that the resistance of the GTO films can be controlled by optimization of the dilution gas flow.

Besides the mist CVD method, the research group also reported GTO thin films fabricated using RF magnetron sputtering. Kato et al. [21] evaluated the optical transmittance and sheet resistance of GTO thin films deposited at different deposition pressures (0.6–7.0 Pa) and Ga:Sn ratios (1:3, 3:1). The results of the GTO thin film deposited at a Ga:Sn ratio of 1:3 indicated that the optical transmittance was more than 80% while the sheet resistance decreased as the deposition pressure increased. In contrast, the optical transmittance and sheet resistance of the GTO thin film deposited at a Ga:Sn ratio of 3:1 decreased with an increase in the deposition pressure. Thus, they concluded that an increase in Ga content will reduce the transparency of the GTO thin films while the sheet resistance of the GTO thin films will decrease with an increase in deposition pressure. Considering the findings in [21], Takagi et al. [22] fabricated GTO thin films for TFTs using RF magnetron sputtering, where the films were deposited at room temperature without annealing. The GTO thin films were fabricated using a sintered GTO ceramic target having a Ga:Sn ratio of 1:3 and a deposition pressure of 1.5 Pa, while the sputtering gas was a mixture of argon and oxygen. To fabricate the GTO TFT, a bottom-gate top contact TFT structure was implemented, where the gate, insulator, source, and drain were Si, SiO$_2$, Ti, and Au, respectively. The μ_{FE}, S, and V_{th} were found to be 0.48 cm^2·V^{-1}·s^{-1}, 1.37 V·dec^{-1}, and 2.22 V respectively. Matsuda et al. [23] extended the study by fabricating amorphous Ga–Sn–O (a-GTO) TFT. The sputtering conditions and TFT structure [22] are as follows. The a-GTO was fabricated by RF magnetron sputtering without annealing using a GTO ceramic target

having a Ga:Sn ratio of 1:3. The thin films were deposited at room temperature. The deposition pressure was varied (0.75, 1, 1.5, 2 Pa) and the TFT structure was a bottom-gate type. The results showed that the μ_{FE} was highest (0.83 $cm^2 \cdot V^{-1} \cdot s^{-1}$) at a deposition pressure of 1.5 Pa while the S was 1.31 $V \cdot dec^{-1}$, and the I_{on}/I_{off} was roughly 10^6. These characteristics render the a-GTO TFT sufficient for AMLCDs with a low switching frame rate, where the V_{th} was 3.27 V. The a-GTO TFT is a normally-off transistor, which is convenient for various practical uses.

Realizing that flat panel displays with a higher frame rate (240 Hz) require a higher μ_{FE}, Matsuda et al. [3] re-fabricated TFTs with a similar structure as in [23], but with the addition of post-annealing. A sintered GTO ceramic target (99.99%, Ga:Sn ratio of 1:3) was used. The vacuum chamber was evacuated to 1×10^{-4} Pa and the sputtering gas pressure was controlled using a vacuum valve to introduce argon and oxygen into the chamber at a fixed flow rate of Ar:O_2 (20:1 sccm). The flow rate was monitored by a mass flow controller. Post-annealing in air was performed at 350 °C for 1 h using an annealing furnace. The X-ray diffractogram revealed that the GTO thin films had an amorphous structure, and the GTO thin films showed good transparency as their absorbance was less than 20% at a wavelength of 300 nm and ~0% above 380 nm. The following characteristics were obtained: (1) I_{on}/I_{off} > 10^8, (2) V_{th} = −1.49 V, (3) S = 0.33 $V \cdot dec^{-1}$, and (4) maximum μ_{FE} = 25.6 $cm^2 \cdot V^{-1} \cdot s^{-1}$. Only a negative shift of 4.3 V was observed after applying negative bias illumination stress (NBIS) conditions with a gate voltage of −20 V under visible light illumination for 3,600 s, which was superior to the characteristics for IGZO TFTs. In addition, no degradation of S was observed in the sub-threshold region of gate-source voltage (V_{gs}) (between −10 V and 5 V) after the NBIS test. The results suggest the possibility of using a-GTO, which is an In-free amorphous metal oxide semiconductor, for TFTs.

Dang et al. [24] fabricated a-GTO thin films on quartz glass placed in an argon-filled chamber using direct current (DC) magnetron sputtering. The target was a ceramic mixture target (85% of SnO_2 and 15% of Ga_2O_3). The a-GTO thin film was deposited at room temperature with a working pressure of 2×10^{-3} Torr. The n-type a-GTO film was found to have the following electrical properties: (1) resistivity: 2.40 $\Omega \cdot cm$, (2) mobility: 2.62 $cm^2 \cdot V^{-1} \cdot s^{-1}$, and (3) carrier density: 1×10^{18} cm^{-3}.

2.4 Deposition methods

Two types of deposition methods will be explained in this section: (1) vacuum deposition and (2) solution-processing deposition.

Magnetron sputtering is the method commonly used to fabricate thin films in vacuum environment. In this method, a suitable gas such as argon is pumped into a vacuum chamber until a designated pressure is reached. Then, current is applied to the target (e.g., metal oxides), resulting in the release of electrons from the target. This results in electrical discharge of argon gas, where the electrons of argon near the target are knocked out by the electrons from the target, producing argon cations (Ar^+). The high-energy cations are attracted to the negative-charged target and the cations bombard the target. The bombardment knocks off atoms from the surface of the target and creates secondary electrons, which leads to argon ionization, repeating the bombardment process [25]. As a result, the bombardment produces scattering sputtered particles of the target, which are then coated onto the substrate, forming a thin film.

In magnetron sputtering, current is applied to the target. There are two types of magnetic sputtering: (1) alternating current (AC) and (2) direct current (DC). The magnetron sputtering method is called RF magnetron sputtering if the applied current is AC. If the injecting current is DC, the method is known as DC magnetron sputtering. Both methods can be used for mass production of thin films over large areas.

Vacuum deposition methods require multiple photolithographic steps as well as sophisticated equipment and operation, resulting in high production cost. Hence, solution-processing deposition can help reduce the production cost because of its simplicity, where it only requires atmospheric environment during film formation. In addition, this method allows deposition of thin films over large areas [7][26]. In general, film formation by solution-processing method is achieved through three steps: (1) coating (e.g., spin-coating), (2) printing (e.g., ink jet) or chemical bath deposition of an aqueous solution onto the substrate, and (3) annealing in air. The metal oxide solution is initially prepared with a soluble precursor or nanoparticles dispersed in a solvent. Liquid thin film is formed since the solvents are volatile, but the liquid thin film changes into a solid thin film by reaction between moisture from the air and metal ligands [7]. In mist CVD, the material solution is transformed into a mist by an oscillator, which differs from the solution-processing method. Following this, the mist is moved into the reactor by a carrier gas, where it finally reacts

through thermal decomposition. The equipment set-up for mist CVD is simple and the method does not require a vacuum condition. In addition, mist CVD is a low cost and environmentally safe method [19].

2.5 Principle of field-effect transistor

Field-effect transistor (FET) is a three-terminal (source, drain and gate) semiconductor device. FET is a voltage-controlled device that controls the flow of current between source and drain, by applying voltage to the gate. Generally, the construction of an FET consists of a channel (either n-channel or p-channel), where two junctions are formed at the ends of the designated channel (either p-n or n-p junctions), depending on the type of FET, as shown in Figure 2.1.

(a)   (b)
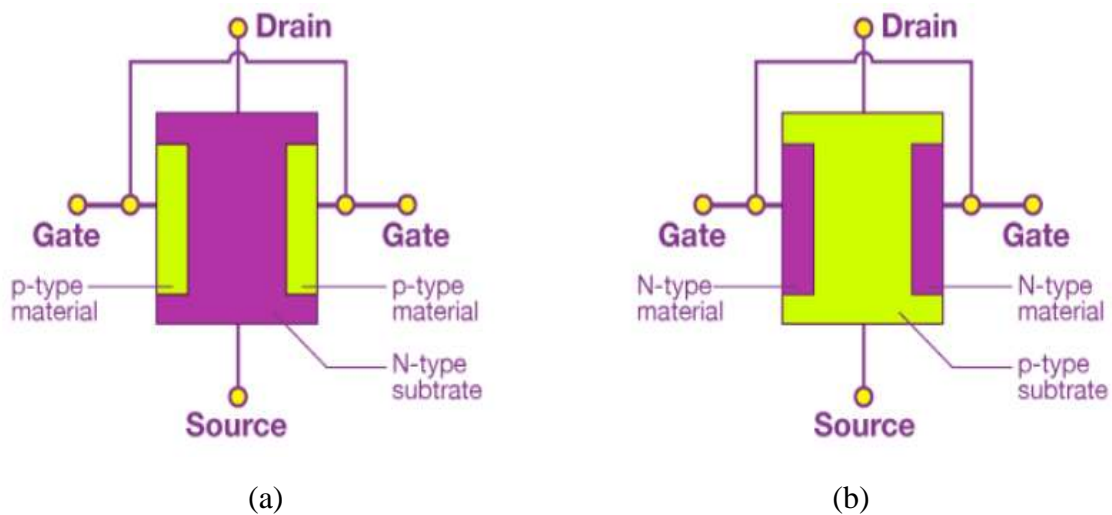
Figure 2.1: Typical construction of FET: (a) n-channel FET, and (b) p-channel FET [27]

When a voltage is applied to the gate, it creates an electric field that affects the width of the depletion region in the channel. The depletion region is the area around the junctions where there are no free charge carriers. If the depletion region is wide, then the resistance of the channel is high, and little current flows between the source and drain. However, if the depletion region is narrow, then the resistance of the channel is low, and more current flows between the source and drain. Therefore, the amount of current that flows between the source and drain is controlled by the voltage applied to the gate.

2.6 Principle of diode

It can be notice that at the ends of the designated channel (refer Figure 2.1), two junctions are formed. The junctions are either p-n or n-p junctions. These junction is similar to a diode. A diode is made of p-type and n-type materials as shown in Figure 2.2.
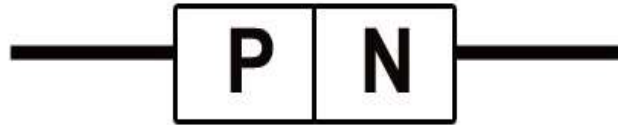
Figure 2.2: Typical construction of diode [28]

The p-type material has an excess of holes; positively charged carriers. While the n-type material has an excess of electrons; negatively charged carriers. When a diode is in forward bias (positive of voltage source is connected to p-type material), the holes in the p-type region are attracted to the electrons in the n-type region, creating a current that flows from the p-type region to the n-type region. However, if a diode is in reversed bias (negative of voltage source is connected to p-type material), the holes in the p-type region are repelled by the electrons in the n-type region, preventing any current from flowing. Therefore, a diode is a two-terminal electronic component that allows current to flow in only one direction (rectifying characteristics), where the typical I–V characteristics of a diode is as shown in Figure 2.3.
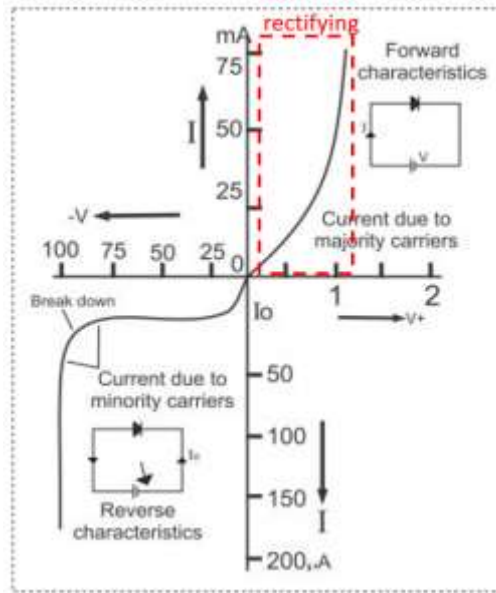
Figure 2.3: I–V characteristics of a diode [28]

2.7 Summary

Due to the scarcity of In in the future, efforts have been made to fabricate In-free semiconductors (GTO thin films) for TFTs by RF magnetron sputtering [3][21][22][23] and DC magnetron sputtering [24]. However, the a-GTO fabricated by Dang et al. [24] using DC magnetron sputtering is focused on a specific Ga:Sn ratio, and this opens avenues for further research using other Ga:Sn ratios. Hence, in this study, GTO thin films were fabricated by DC magnetron co-sputtering. The Ga:Sn ratio was adjusted by varying the (1) current applied to the targets and (2) number of Ga_2O_3 pellets. Following this, the composition, phase, and optical transmittance of the GTO thin films were characterized. Furthermore, the current–voltage (I–V) characteristics of the fabricated ITO/GTO bilayer diode thin films were also determined.

CHAPTER 3

METHODOLOGY

3.1   Experimental set-up

In this study, an opposed-target DC magnetron sputtering system was used to fabricate the junction films. The experimental parameters were the same as those used in the literature by Professor Toshihiro Moriga's research team in Tokushima University [29][30][31][32]. The schematic diagram of the DC magnetron co-sputtering system is shown in Figure 3.1.
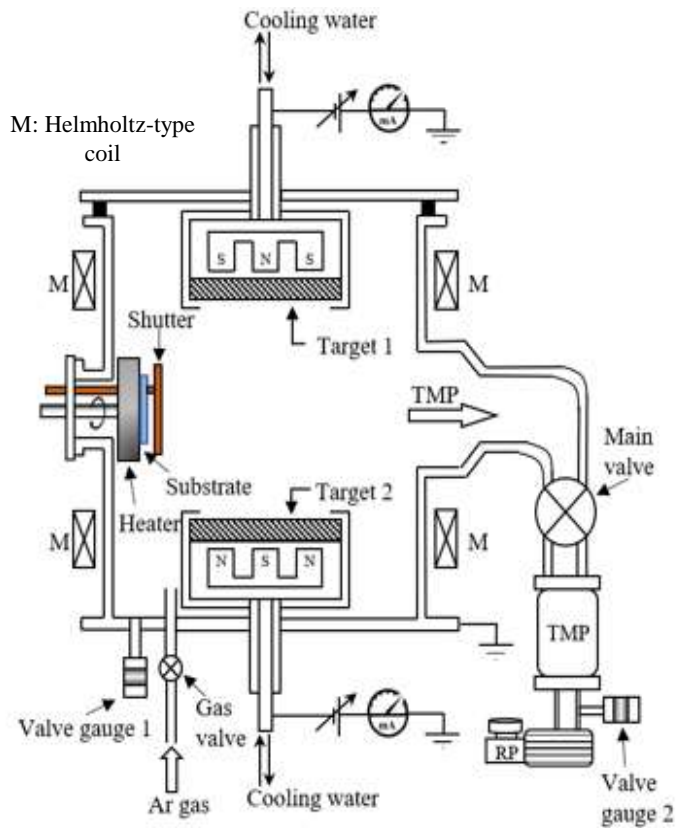
Figure 3.1: Schematic diagram of the DC magnetron co-sputtering system

3.2   Fabrication of transparent In–Sn–O/Ga–Sn–O (ITO/GTO) bilayer thin films

To fabricate the ITP/GTO bilayer thin films, the ITO thin film was first deposited, followed by the deposition of the GTO thin film at designated positions on the ITO thin film. The ITO thin film was deposited onto a glass substrate by DC magnetron co-sputtering

system using a SnO_2 ceramic disc (Target 1, set at the 12 o'clock position) facing an In_2O_3 ceramic disc (Target 2, set at the 6 o'clock position). The glass substrate (Corning® #7059 barium-borosilicate glass) was placed at the 9 o'clock position and rotated at a constant rate of 10 rpm in order to obtain a uniform thin film surface. All targets have a diameter of 100 mm. A magnetic field was applied to the chamber by using coils outside the equipment. The current applied to the SnO_2 target and the In_2O_3 target was 12 and 48 mA, respectively, such that the ITO thin film formed had an In:Sn ratio of ~9:1. The ITO thin film was deposited in pure argon (sputtering gas) at a working pressure and exhaust pressure of 0.2 and 5.0 Pa, respectively, for 3 h. In order to achieve a pure argon gas environment, the atmospheric pressure in the vacuum chamber was initially reduced to 1.3×10^{-3} Pa. Following this, argon was gradually introduced into the vacuum chamber until the pressure reached 13 Pa. Next, adjustments by exhaustion were made to meet the required working pressure and exhaust pressure. Prior to sputtering, the glass substrate was ultrasonically cleaned with acetone and rinsed with ethanol. The glass substrate was then placed onto a substrate holder without rotation. Before film formation, pre-sputtering was carried out for 1 h. During this period, the dust on the surfaces of both targets was removed while the substrate was protected behind a shutter.

GTO thin films were deposited at an appropriate position on the ITO thin film by DC magnetron co-sputtering of a SnO_2 target (Target 1) facing a SnO_2 target (Target 2) containing Sb (10%). Furthermore, a number of Ga_2O_3 pellets was placed on the erosion region of Target 2. Both Target 1 and Target 2 have a diameter of 100 mm. The Ga_2O_3 pellets are disc-shaped with a diameter of 10 mm. The Ga_2O_3 pellets were used to vary the Ga content in the GTO thin films. The number of Ga_2O_3 pellets to be simultaneously sputtered with respect to one type of thin film was defined as 'n' and varied from 2 to 3 ($n = 2$ and 3). The arrangement of the Ga_2O_3 pellets is shown in Figure 3.2.
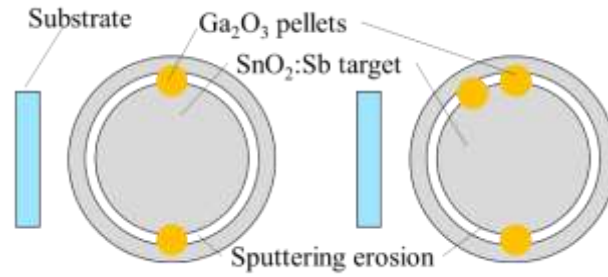
Figure 3.2: Position of the Ga_2O_3 pellets on the erosion region of Target 2

The currents applied to both targets were controlled independently. Two conditions were considered. In the first condition, the currents applied to Target 1 and Target 2 were 0 and 60 mA, respectively (0–60 mA), whereas in the second condition, the currents applied to Target 1 and Target 2 were 10 and 50 mA, respectively (10–50 mA). The deposition was carried out for 30 min in pure argon, where the working pressure and exhaust pressure were 0.2 and 2.5 Pa, respectively. Pre-sputtering was carried out for 1 h before film formation. During this period, the dust on the surfaces of both targets was removed while the substrate was protected behind a shutter. Four samples were prepared in this study. Each sample was prepared according to the temperature of the glass substrate during deposition of the ITO/GTO bilayer thin films, as summarized in Table 3.1.

Table 3.1: Samples prepared in this study based on the temperature of the glass substrate during deposition of the ITO/GTO bilayer thin films

Sample	First layer (ITO)	Second layer (GTO)	After deposition
Sample 1	*RT	RT	None
Sample 2	200 °C	RT	None
Sample 3	200 °C	RT	Anneal
Sample 4	200 °C	200 °C	None

*Note: RT denotes room temperature.

Annealing was performed at room temperature, followed by setting the current applied to each target to zero and subsequently increasing the substrate temperature to 200 °C for 1 h after deposition.

3.3   Characterization

This sub-chapter is focused on the methods used to characterize the GTO thin films: (1) elemental composition, (2) structure, (3) optical transmittance, (4) surface profile. The *I–V* characteristics of the ITO/GTO bilayer thin films were also determined.

3.3.1   Elemental analysis using wavelength-dispersive X-ray (WDX)

In wavelength-dispersive X-ray (WDX) spectroscopy, the specimens and spectroscopic crystal detectors have optical characteristics that satisfy Bragg's law. Characteristic X-rays (fluorescent X-rays) generated by irradiating X-rays onto a specimen are spectrally separated by a spectroscopic crystal and scattered through a slit into scintillation detectors (mainly for light) and gas flow detection proportional counters (mainly for elements). The signal from the detector is amplified and the signal is then sent to a computer for data processing and analysis. Noise and unnecessary signals are removed by a wave height analyser. WDX spectroscopy enables accurate analysis of a wide range of elements.

In this study, Pd ceramic target was used as the X-ray source while lithium fluoride (LiF) and PET were used as the spectroscopic crystals. A high-power benchtop sequential wavelength-dispersive X-ray fluorescence spectrometer (Supermini200, Rigaku Corporation), was used for the analysis, where the instrument can qualitatively and quantitatively analyse elements in thin films in a non-destructive, accurate, and quick manner.

3.3.2 Structural analysis using X-ray diffraction analysis

Most of the materials in materials science are solids, which are composed of three-dimensional arrangement of atoms, molecules, or ions in a regular, repeating fashion. This arrangement influences the properties of solids. Hence, if a material is composed of a regular array of units, only unit needs to be examined in detail and it will be representative of the whole material due to the repeating pattern of atoms, molecules, or ions.

X-ray is a type of electromagnetic wave with a wavelength of ~ 0.1 Å and high energy of ~100 keV. When a material is irradiated with X-rays, scattering and diffraction occur, where some are absorbed to generate fluorescent X-rays and the rest is transmitted. There

are three types of X-ray analysis: (1) X-ray transmission analysis, (2) X-ray spectroscopy, and (3) X-ray diffraction analysis. These methods are collectively called X-ray analysis.

Diffraction phenomenon is related to the atomic arrangement of a substance, where light interacts with a substance whose atoms are arranged regularly like crystals. The angle of incidence of X-rays at which diffraction occurs is determined by the crystalline structure of the material. Powder X-ray diffraction is widely used because it can obtain information on the crystalline structure and phases of a material in a non-destructive manner. The X-ray diffraction in thin films has a length that is close to the wavelength of the visible light in the thickness direction. The X-rays penetrate through the thin film from the low angle and then the X-rays are scattered by the substrate. For this reason, structural analysis of the thin films was conducted in a mode called parallel beam measurement. This mode can measure the incident X-rays at a fixed low angle irrespective of thin film shape. When X-rays strike a substance and are scattered, their wavelength may be the same as the wavelength of the incident X-ray or the energy may be attenuated due to interactions with the solid. The former case is called Rayleigh scattering, which interferes with each other and causes a diffraction phenomenon, whereas the latter case is called Compton scattering, where no interference occurs.

For a model in which the lattice plane is regarded as a translucent specular surface, let us consider the interplanar spacing d [Å] of the intervals between the crystal planes aligned in parallel. The incidence angle and the reflection angle of X-rays for each plane are denoted by θ. In order to cause the diffraction phenomenon due to Rayleigh scattering, the length of the difference ($2d \sin \theta$) in the optical path length of X-rays incident on another crystal plane equivalent to a certain crystal plane is an integer multiple of the wavelength λ of the incident X-rays. At this time, the diffraction phenomenon occurs because the phases of the scattered wave from the adjacent crystal face and the incident wave are aligned and strengthened. This is called Bragg's law. When the substance to be observed is a crystal, a diffraction pattern consisting of discontinuous sharp peaks corresponding to regular periodicity of atomic arrangement is observed.

However, for amorphous materials, the crystal structure does not have a regular arrangement of atoms, molecules, or ions, and the light reflected from each atom does not cause interference. This strengthens the peak broadly and the intensity decreases. In this study, XRD analysis was carried out not only to analyse the structure of the thin films

immediately after film formation, but also to analyse the structure of the GTO thin films after the number of Ga$_2$O$_3$ pellets was changed.

An X-ray diffractometer (Model: SmartLab, Rigaku Corporation) using Cu Kα radiation ($\lambda = 1.5418$ Å) as the X-ray source was used in this study. The measurements were carried out within a scanning range of 20–80° at a voltage of 30 kV, tube current of 100 mA, scanning speed of 4°/min, and scanning step width of 0.02°.

3.3.3 Optical transmittance analysis using ultraviolet–visible (UV–VIS)

The optical transmittance of the GTO thin films was measured using an UV–VIS spectrophotometer (Model: V-670, JASCO Inc.) The instrument uses a deuterium lamp (200–350 nm) and halogen lamp (330–900 nm), where the measurement is carried out over the entire UV–VIS wavelength range of 200–900 nm. In general, the light transmittance of a substance is expressed as the ratio of light intensity between the light incident on a substance and the light transmitted through a substance, as given by Equation 3.1:

$$I = I_0 e^{-ax} \tag{3.1}$$

where I is the incident light intensity, I_0 is the transmitted light intensity, a is the absorption coefficient, and d is the film thickness. The film thickness is estimated from the optical interference observed between the thin film and substrate, while a is calculated using Equation 3.2:

$$a = -\frac{1}{d} \cdot ln\left(\frac{I}{I_0}\right) \tag{3.2}$$

The bandgap (E_g) of a material is determined from the Tauc plot, which is plotted based on Equation 3.3:

$$(ahv)^{1/m} = k\left(hv - E_g\right) \tag{3.3}$$

where h is Plank's constant and m is the semiconductor state.

The $(ahv)^2$ versus hv plot [33] shows the position of the absorption edge. With the appropriate auxiliary line, the value of E_g can be estimated. While measuring the light transmittance of a thin film, a vibration waveform will appear depending on the wavelength, because light in a thin film with a thickness in the range of nanometres (nm) is reflected, causing interference. In this study, the visible light transmittance is the arithmetic mean of each transmittance wavelength in the visible light region.

3.3.4 Surface profile analysis using atomic force microscope

In this study, an atomic force microscope was used to examine the structure and growth process of the thin film surface. The atomic force microscope measures the gravitational or repulsive force from the deflection of the cantilever (minute leaf spring). The instrument images the surface by scanning the needle along the surface. The Lennard–Jones potential is given by Equation 3.4:

$$V(r) = 4\varepsilon\left\{\left(\frac{r_0}{r}\right)^{12} - \left(\frac{r_0}{r}\right)^{6}\right\} \tag{3.4}$$

At long distances $(r > r_0)$, the gravitational potential due to the Waals force (represented by $-1/Z^6$) is predominant, whereas at close distances $(r < r_0)$, the repulsive force potential explained by Pauli's exclusion law (represented by $+1/r^{12}$) is predominant. Atomic force microscope can directly measure the force acting between atoms, where each force is based on Newton's second law of motion. The force acting between atoms is given by Equation 3.5:

$$F = -\frac{dV(r)}{dr} = \frac{24\varepsilon}{r_0}\left\{2\left(\frac{r_0}{r}\right)^{13} - \left(\frac{r_0}{r}\right)^{7}\right\} \tag{3.5}$$

The point with the maximum attractive force is the distance r_0 at which $dF/dr = 0$ by further differentiating the above equation. In atomic force microscopy, the repulsive force can be determined by simply bringing the probe and the sample surface into contact.

In this study, the surface profiles of the thin films were observed using an atomic force microscope (Model: Nanopics 2100, NanoTechnology, Inc.). The surface profiles of the thin films formed on the glass substrates were primarily measured in contact mode.

3.3.5   I–V characteristics

The current–voltage (I–V) characteristics of the ITO/GTO bilayer thin films were determined by using the circuit shown in Figure 3.3. The circuit consists of a programmable DC voltage/current generator (Model: Advantest R6144), a resistor (500 Ω), a digital pico-ammeter, and a diode. It shall be noted that the voltage supply of the programmable DC voltage/current generator used in this study is within a range of −20–20 V, with a 1-V interval. The diode symbol in Figure 3.3 denotes the ITO/GTO bilayer thin film.
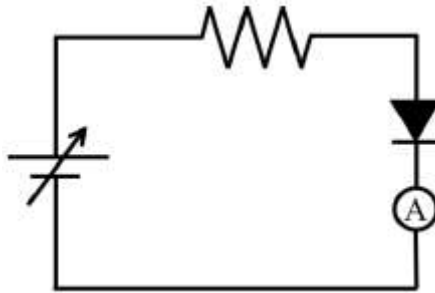
Figure 3.3: Circuit used to measure the I–Vcharacteristics of the ITO/GTO bilayer diode thin films

CHAPTER 4

RESULTS AND DISCUSSION

4.1   Elemental compositions of the GTO thin films

The elemental compositions of the GTO thin films deposited at room temperature and 200 °C were determined using WDX spectroscopy, and the results are tabulated in Table 4.1 and Table 4.2. It can be seen that the Ga:Sn ratio increased with an increase in the applied current of Target 2 and number of Ga_2O_3 pellets. The Ga:Sn ratio significantly decreased as the substrate temperature increased. The increment of Ga content is due to a higher electric field (increment of the applied current) applied to Target 2 and the number of Ga_2O_3 pellets that caused more atoms to be sputtered off Target 2 onto glass substrates. However, the decrement of Ga content as the substrate temperature increased (from room temperature to 200 °C) might be due to thermal diffusion because as deposition temperature increases, the atoms gain more energy which also could lead the atoms to diffuse from each other resulting in loss of gallium atoms from the films.

Table 4.1: Elemental compositions of the GTO thin films deposited onto glass substrates at room temperature

Number of Ga_2O_3 pellets and applied current	Ga content (mol%)	Sn content (mol%)
$n = 2$, 0–60 mA	28.0	72.0
$n = 2$, 10–50 mA	24.5	75.5
$n = 3$, 0–60 mA	38.0	62.0
$n = 3$, 10–50 mA	35.0	65.0

Table 4.2: Elemental compositions of the GTO thin films deposited onto glass substrates at 200 °C

Number of Ga_2O_3 pellets and applied current	Ga content (mol%)	Sn content (mol%)
$n = 2$, 0–60 mA	20	80
$n = 2$, 10–50 mA	18	82
$n = 3$, 0–60 mA	25	75
$n = 3$, 10–50 mA	24	76

4.2   Structures of the GTO thin films

Figure 4.1 shows the X-ray diffractograms of the GTO thin films sputtered at 200 °C (Figure 4.1A) and GTO thin films annealed at 200 °C after deposition at room temperature (Figure 4.1B).

(A)

(B)
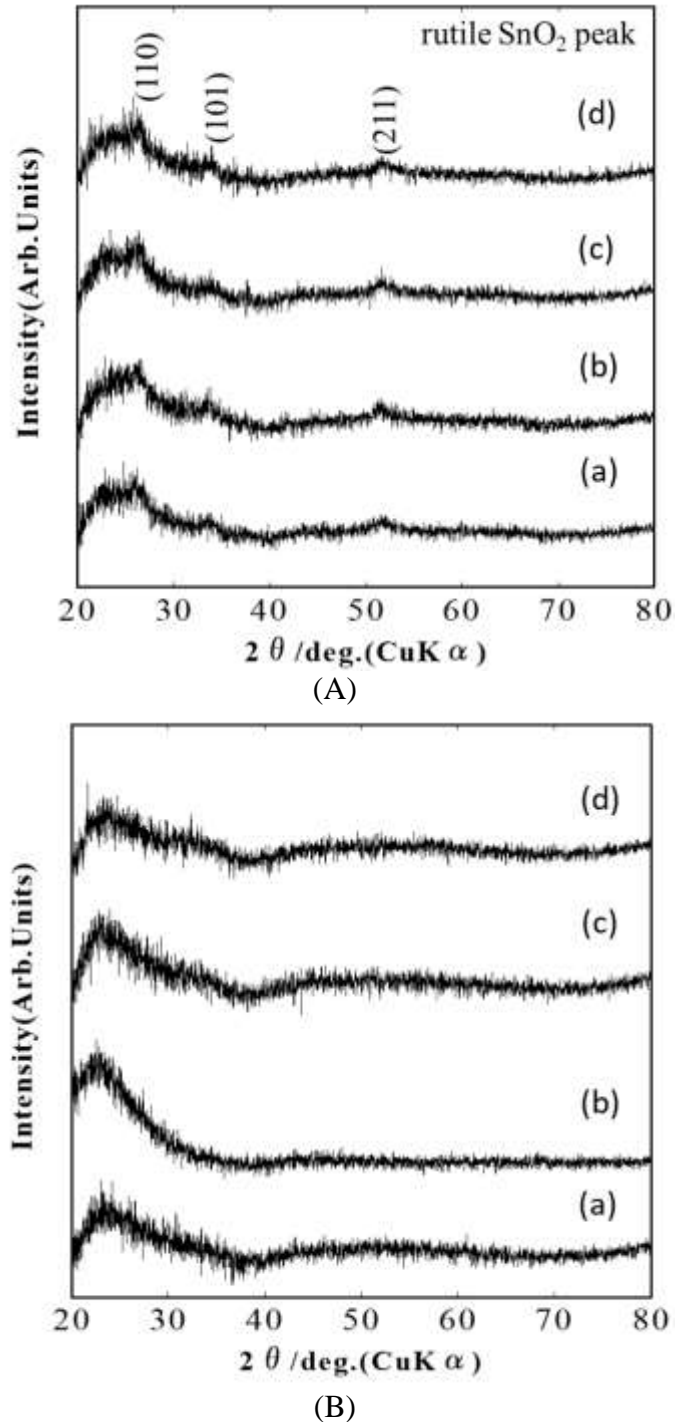
Figure 4.1: X-ray diffractograms of the (A) GTO thin films sputtered onto glass substrates at 200 °C and (B) GTO thin films annealed at 200 °C after deposition onto glass substrates at room temperature.
(a) $n = 2$, 10–50 mA, (b) $n = 2$, 0–60 mA,
(c) $n = 3$, 10–50 mA, (d) $n = 3$, 0–60 mA

It can be observed from Figure 4.1A, small intensity peaks appeared at 2θ of 26.3, 33.8, and 52.0°. In contrast, it can be observed from Figure 4.1B that broad peaks appeared (which were attributed to glass), indicating that the GTO thin films had an amorphous structure. The three peaks observed in Figure 4.1A correspond to SnO_2 having a rutile structure. This is thought to be due to the difference in the method of heating the GTO thin films, i.e., whether the GTO thin films were prepared by sputtering on heated ITO thin films or the GTO thin films were annealed at 200 °C after they were deposited at room temperature.

The X-ray diffractograms of the GTO thin films sputtered onto heated ITO are shown in Figure 4.2A and the X-ray diffractograms of the GTO thin films annealed at 200 °C after deposition onto heated ITO at room temperature are shown in Figure 4.2B

It can be seen from both profiles (Figure 4.2A and Figure 4.2B) that sharp peaks attributed to ITO appeared. The presence of peaks at ~26.3 and 37.6° can be confirmed for the GTO thin films sputtered at 200 °C, unlike the annealed GTO thin films. Since the method of film formation on the ITO thin films is the same, the difference between these peaks is thought to be due to the difference in heat treatment (annealing) of the GTO thin films, as shown in Figure 4.1. In addition, the peak at ~37.6° in Figure 4.2A appeared only for the GTO thin films with a Ga content of more than 24 mol%. The (110) and (200) planes include body-centred cations, which dominate the octahedral site in the rutile structure. It is thought that the sputtering process at 200 °C increases crystallinity of the GTO thin films based on rutile SnO_2 and increasing the Ga donation (e.g., $n = 3$) with sputtering promotes substitution from Sn to Ga, resulting in the (200) plane. It is thought that the crystallinity of the GTO thin films also differs depending on the Ga content.
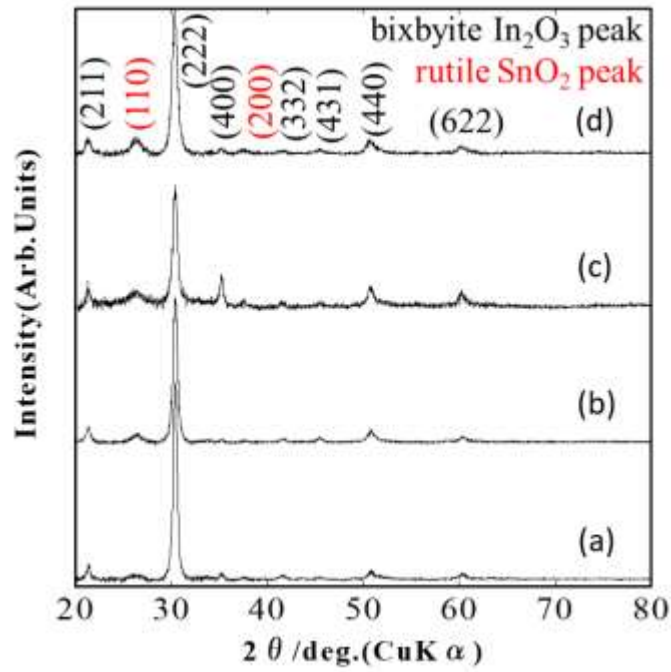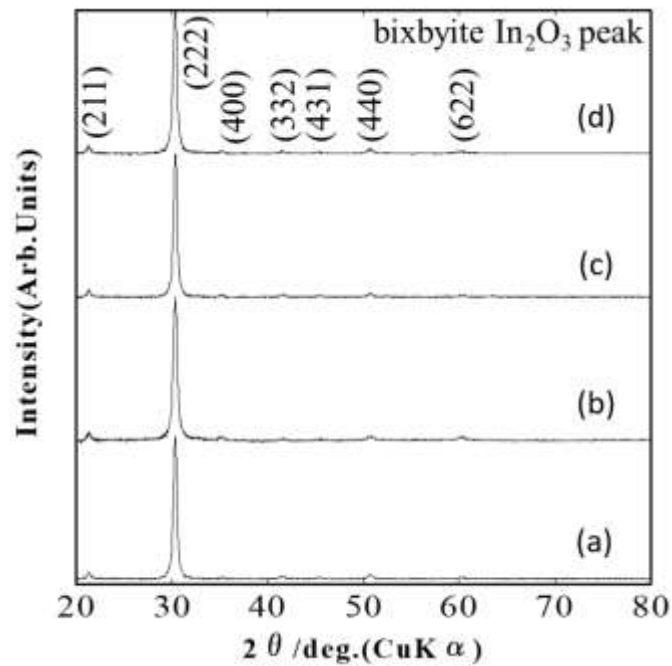
Figure 4.2: X-ray diffractograms of the (A) GTO thin films sputtered onto heated ITO thin films at 200 °C and (B) GTO thin films annealed at 200 °C after deposition onto heated ITO thin films at room temperature.
(a) $n = 2$, 10–50 mA, (b) $n = 2$, 0–60 mA,
(c) $n = 3$, 10–50 mA, (d) $n = 3$, 0–60 mA

Figure 4.3 shows the results of the Seebeck measurement of the GTO thin films. It can be seen that the Seebeck coefficient did not change systematically with the furnace temperature. The Seebeck coefficient varied for the annealed GTO thin films and thus, the type of carrier could not be identified.
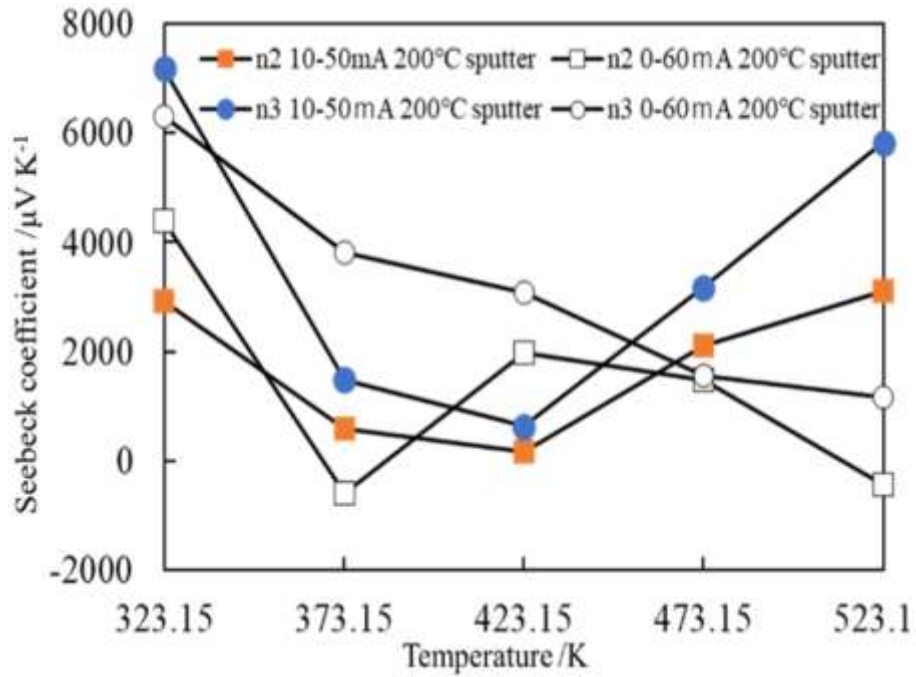
(A)
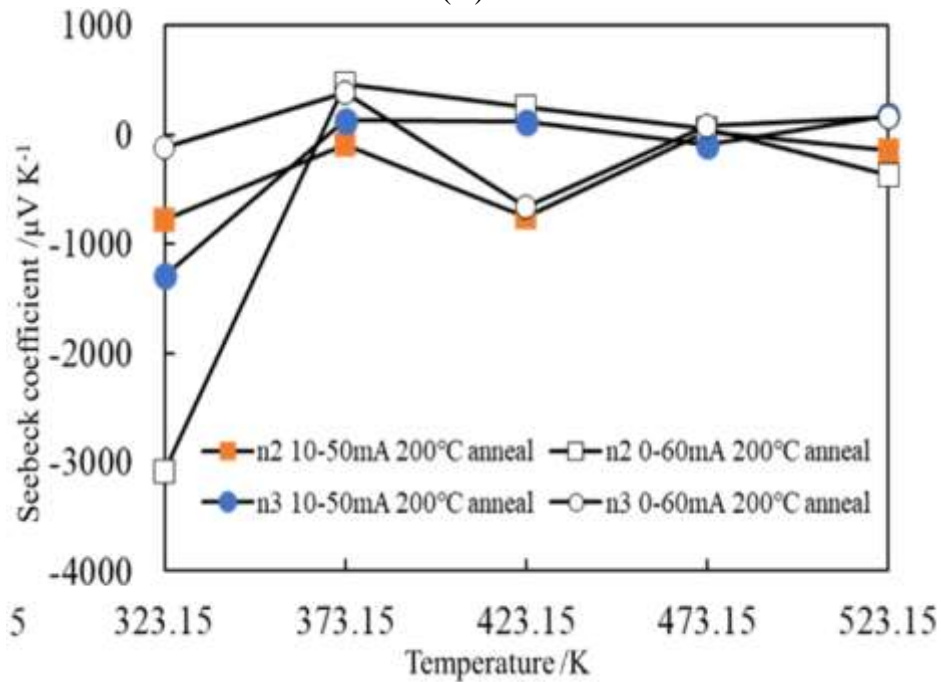
(B)

Figure 4.3: Seebeck coefficients of the (A) GTO thin films sputtered at 200 °C and (B) GTO thin films annealed at 200 °C after deposition at room temperature

On the other hand, the Seebeck coefficients were positive and stable for the GTO thin films sputtered at 200 °C except for the sample with $n = 2$ and an applied current of 0–60 mA. This suggests that the GTO thin films prepared by sputtering at 200 °C has better diffusion of sputtered particles during film formation compared with the GTO thin films annealed at 200 °C after deposition at room temperature. The GTO thin films become a p-type semiconductor that generates holes by substituting Ga^{3+} for Sn^{4+}, as given by Equation 4.1:

$$Ga_2O_3 \xrightarrow{SnO_2} 2Ga'_{Sn} + 3O_o^x + h + \frac{1}{2}O_2 \tag{4.1}$$

In Figure 4.3A, higher absolute Seebeck coefficients at room temperature were obtained for the samples with $n = 3$. The samples with $n = 3$ have more holes than those with $n = 2$ since the former has higher Ga content than the latter, as confirmed from the elemental analysis. In addition, the samples with $n = 3$ promotes substitution, as indicated by the XRD analysis.

4.3   Optical transmittance of the GTO thin films

UV–VIS transmittance spectra of the GTO thin films sputtered at room temperature GTO films ($n = 2$ and $n = 3$) with respect to the incident light wavelength are shown in Figure 4.4. The average transmittance was more than 80% for all GTO thin films for wavelengths in the visible light region (380–780 nm). It can be seen that there was no significant difference in the transmittance for the GTO thin films with an applied current of 10−50 mA regardless of the number of Ga_2O_3 pellets. The GTO thin films with an applied current of 0−60 mA showed a shift in the absorption edge towards shorter wavelengths. Based on the Tauc plot, the GTO thin films had an optical band gap (E_g) within a range of 3.71–3.75 eV, where the E_g increased as the atomic per cent of % of Ga in the GTO thin films increased.
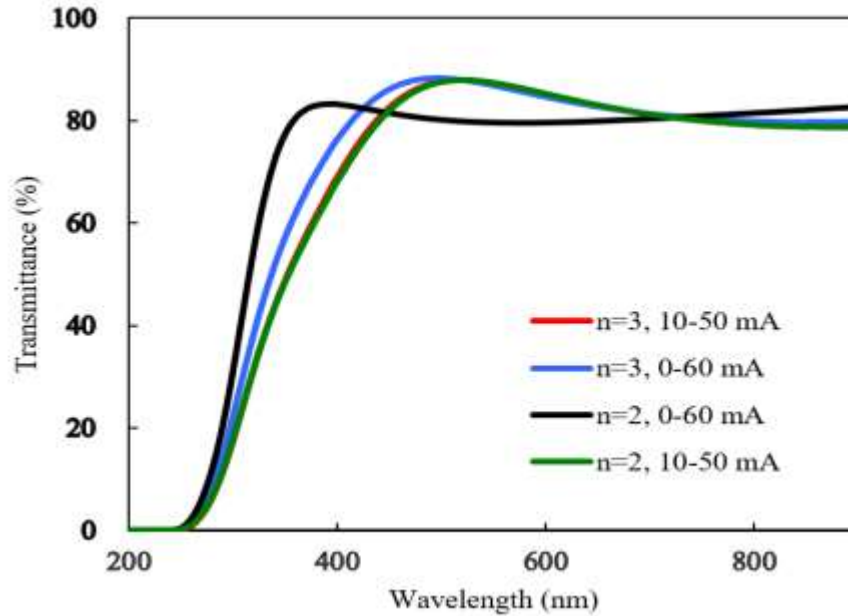
Figure 4.4: UV–VIS transmittance spectra of the GTO thin films sputtered at room temperature

Figure 4.5 shows the UV–VIS transmittance spectra of the GTO thin films sputtered onto glass substrates at 200 ℃. In the visible light region (380–780 nm), the average transmittance of the GTO thin films annealed at 200 ℃ was within a range of 81.8–83.6% whereas the average transmittance of the GTO thin films sputtered at 200 ℃ was within a range of 78.1–80.4%. The difference in the average transmittance is likely due to the increase in crystallinity for the GTO thin films sputtered at 200 ℃, as indicated by the X-ray diffractograms, such that grain boundaries form, which scatter light. The GTO thin films sputtered with an applied current of 60 mA applied showed a slight shift in the absorption edge compared with the GTO thin films sputtered with an applied current of 50 mA. The shift in the absorption edge of the GTO thin films is caused by the Burstein–Moss shift. Since Ga acts as acceptor in the GTO thin films sputtered at 200 ℃, the slight shift in absorption edge is due to the removal of the adsorbate (e.g., water) by heat treatment, which affects the electrical properties of the GTO thin films. It has been reported that hydrogen ions act as donors, which affects the electrical properties of In–Ga–Zn–O thin films.
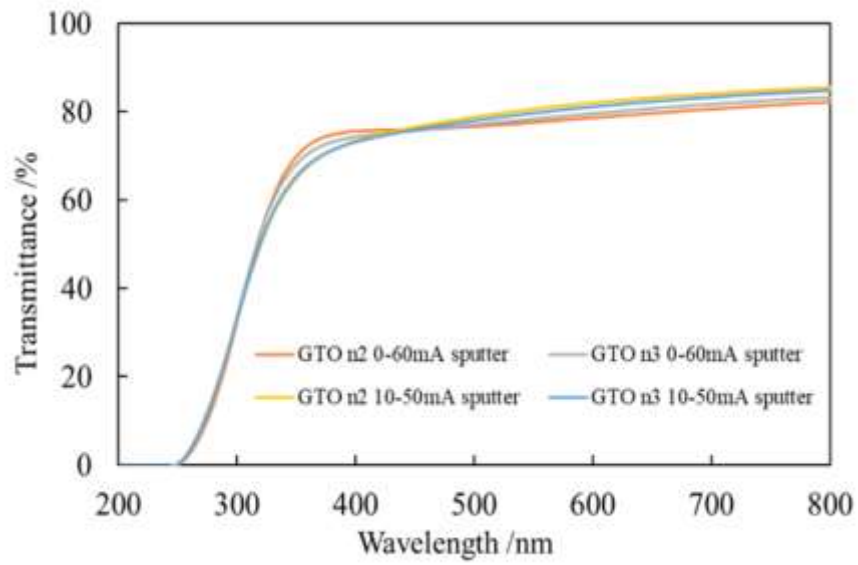
(A)
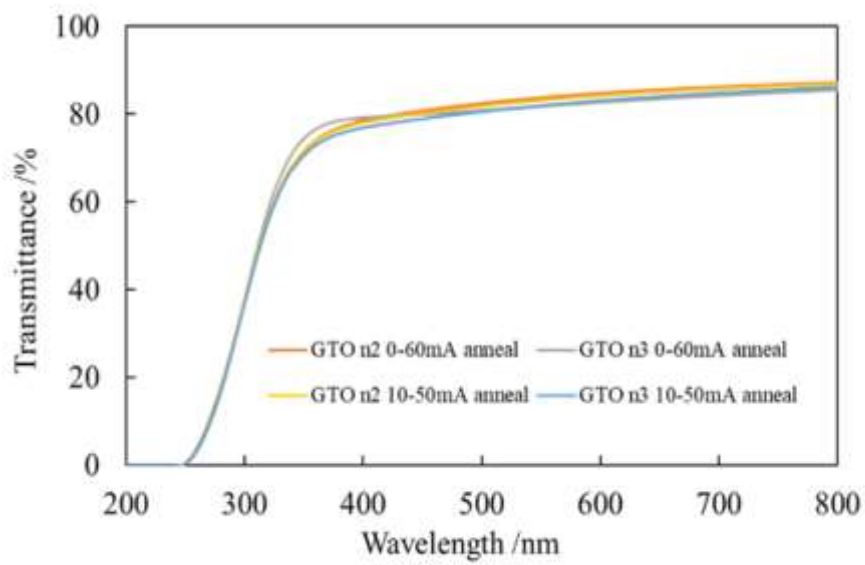
(B)

Figure 4.5: UV–VIS transmittance spectra of the (A) GTO thin films sputtered at 200 ℃ and (B) GTO thin films annealed at 200 ℃ after deposition at room temperature

4.4　Surface profiles of the GTO thin films

The atomic force microscopy images (Figure 4.6) of the ITO/GTO bilayer thin films post-annealed at 200 °C indicate a distinct rectifying behaviour. All of the films were ~10 nm thick. The arithmetic mean surface roughness of each film was ~0.7 nm. The films were smooth, exhibiting ~10% bumpiness relative to the film thickness. No significant differences were observed between the surface textures of the films.

(a)　　　　　　　　　　　　　　　　　(b)

(c)　　　　　　　　　　　　　　　　　(d)
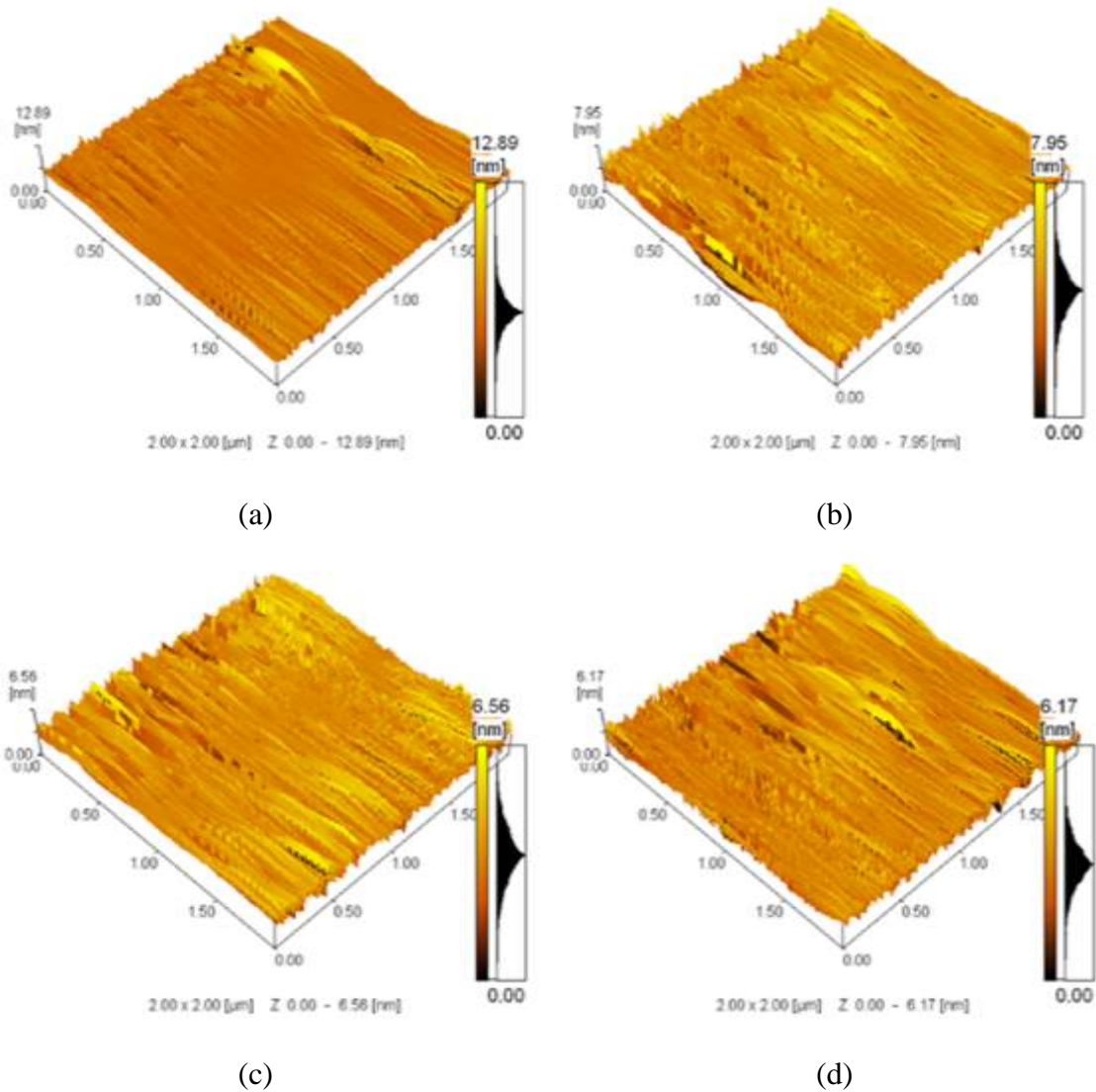
Figure 4.6: Atomic force microscopy images of the ITO/GTO bilayer thin films, where the ITO and GTO thin films were deposited at 200 °C and room temperature, respectively, followed by annealing at 200 °C.
(a) $n = 2$, 0–60 mA, (b) $n = 2$, 10–50 mA, (c) $n = 3$, 0–60 mA, and (d) $n = 3$, 10–50 mA

4.5   I–V characteristics of the ITO/GTO bilayer thin films

Figure 4.7 shows the I–V characteristics of the ITO/GTO bilayer thin films deposited at room temperature.
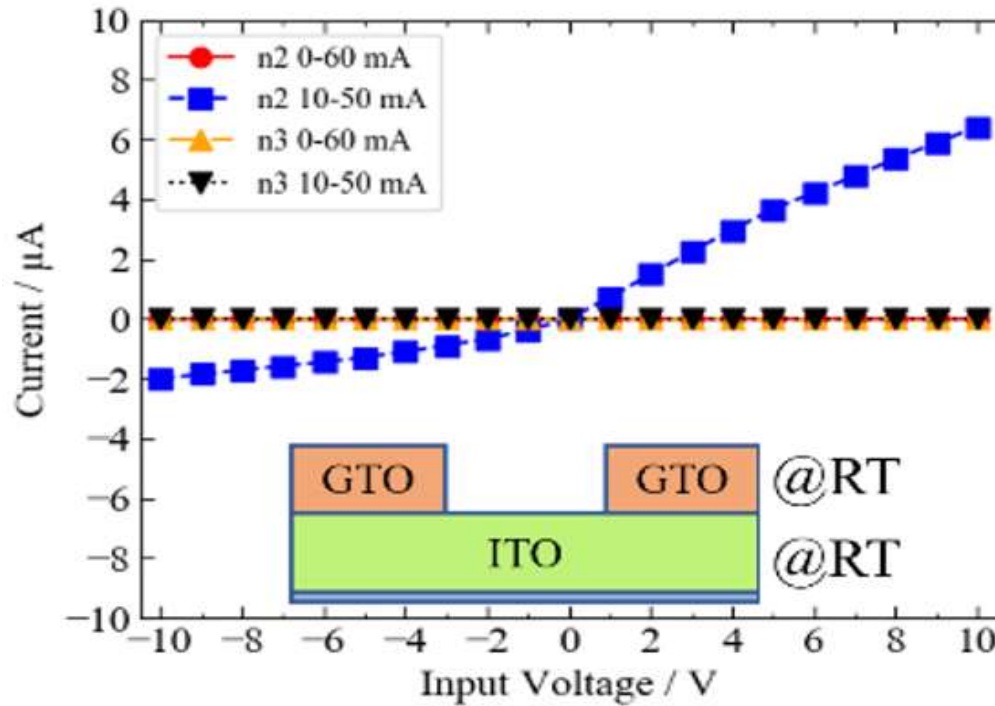
Figure 4.7: I–V characteristics of the ITO/GTO bilayer thin films deposited at room temperature

It can be observed that there was rectifying behaviour with different conductivities between positive and negative voltage supply with 0-V input as the boundary for the sample fabricated with $n = 2$ and an applied current of 10–50 mA. The GTO and ITO thin films act as the anode and cathode, respectively. The other samples showed a linear I–V relationship; however, the samples displayed a significantly high resistivity. The GTO thin film with a Ga content of ~25 mol% deposited at room temperature was found to be suitable to obtain rectifying behaviour. This ratio is reasonable based on the Ga:Sn ratio of 1:3 of the GTO target used in a previous study [3].

Figure 4.8 shows the I–V characteristics of the ITO/GTO bilayer thin films, where the GTO thin films were deposited at room temperature while the ITO thin films were deposited at 200 °C. The sample fabricated with $n = 2$ and an applied current of 0–60 mA showed a nearly voltage-independent behaviour. A rectifying characteristic of 3.80 µA/V was obtained upon the application of positive voltage.
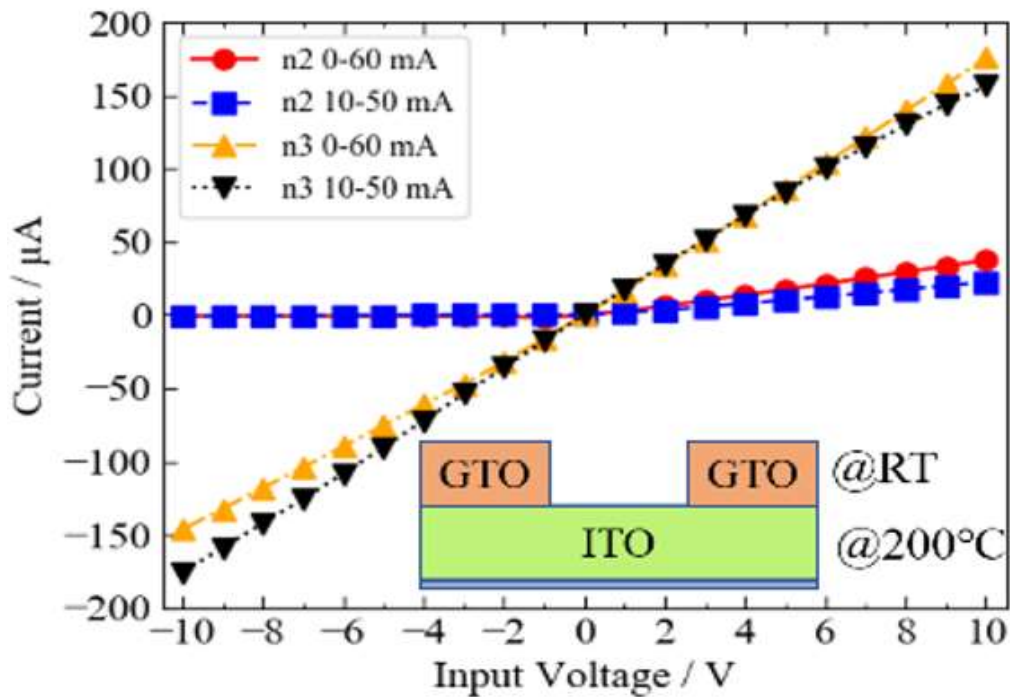
Figure 4.8: I–V characteristics of the ITO/GTO bilayer thin films, where the ITO and GTO thin films were deposited at 200 °C and room temperature, respectively

Figure 4.9 shows the I–V characteristics of the ITO/GTO bilayer thin films, where the GTO thin films were deposited at room temperature whereas the ITO thin films were deposited at 200 °C. The ITO/GTO bilayer thin films were subsequently annealed at 200 °C. Figure 4.9 is similar to Figure 4.8, where rectifying behaviour can be observed in the samples prepared with $n = 2$ whereas ohmic resistive behaviour can be observed in the samples prepared with $n = 3$. All samples in Figure 4.9 exhibited ohmic behaviour. The X-ray diffractograms of the junction films after annealing under the same processing conditions as those of the samples shown in Figure 4.9 demonstrated peaks attributed only to In_2O_3, thereby confirming that the GTO thin films were amorphous.
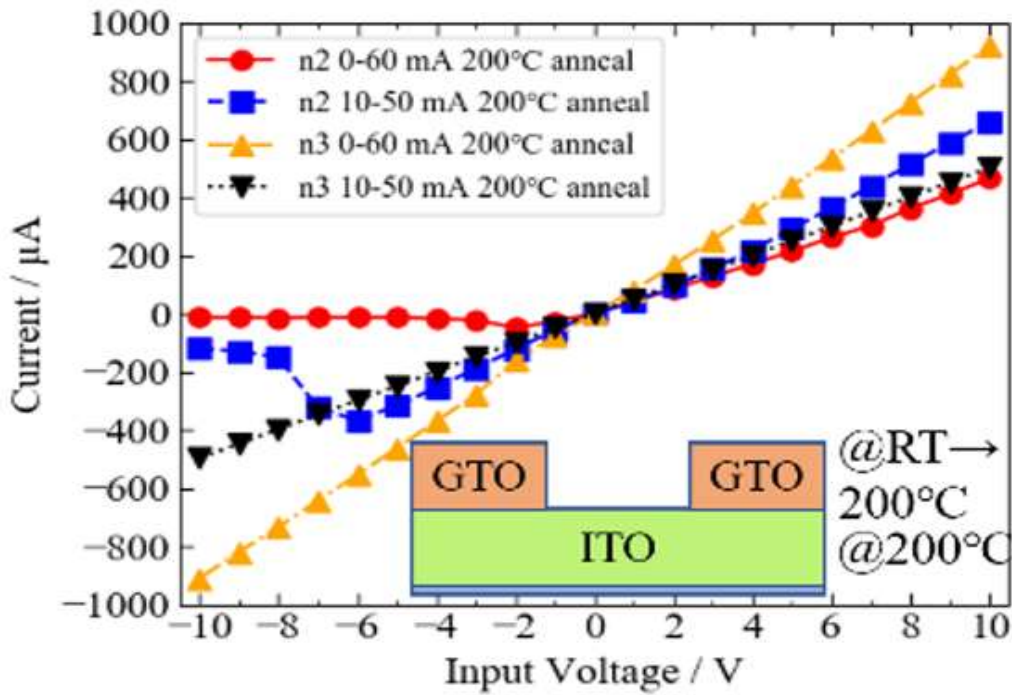
Figure 4.9: I–V characteristics of the ITO/GTO bilayer thin films where the ITO and GTO thin films were deposited at 200 °C and room temperature, respectively, followed by annealing at 200 °C

Figure 4.10 shows the I–V characteristics of the ITO/GTO bilayer thin films; the primary difference being that both GTO and ITO thin films were deposited at 200 °C.
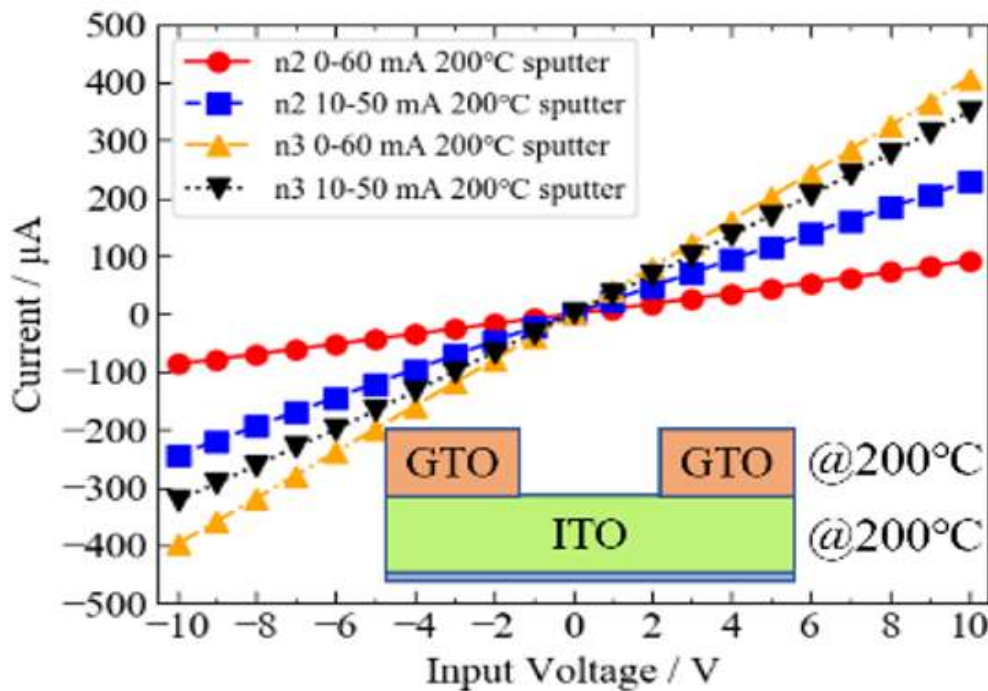
Figure 4.10: I–V characteristics of the ITO/GTO bilayer thin films deposited at 200 °C

However, the X-ray diffractograms of the junction films after heating both GTO and ITO thin films to 200 °C and depositing the films under the same processing conditions as the samples in Figure 4.10 indicate the presence of In_2O_3 and SnO_2. Thus, the samples with $n = 2$ no longer exhibited rectifying characteristics, possibly because of the decrease in the carrier concentration owing to the crystallization of SnO_2. The decrease in carrier concentration can be inferred from the decrease in the average slope of the respective I–V characteristics in Figure 4.9 and Figure 4.10.

The sample prepared with $n = 2$ and an applied current of 10–50 mA (Figure 4.9) had a large reverse current with a maximum value of −370 μA. The sample exhibited minimum current at −6 V because of the reverse bias applied to the film. For the sample with $n = 2$ and an applied current of 0–60 mA, the maximum value of the reverse current was 49 μA at −2 V. The maximum current is approximately one order of magnitude higher in Figure 4.9 than in Figure 4.8, indicating that annealing improves the conductivity. When a positive voltage was applied, rectifying characteristic of 68.3 μA/V was obtained for the sample fabricated with $n = 2$ and an applied current of 0–60 mA while a rectifying characteristic of 46.0 μA/V was obtained for the sample fabricated with $n = 2$ and an applied current of 10–50 mA.

CHAPTER 5

CONCLUSION AND RECOMMENDATIONS FOR FUTURE WORK

5.1 Conclusions

In this study, GTO thin film semiconductors were fabricated by DC magnetron co-sputtering of SnO_2 targets and Ga_2O_3 pellets. The results showed that the GTO thin films had an amorphous structure and an optical transmittance of more than 80% within the visible light region, regardless of the Ga:Sn ratio. Furthermore, diodes with non-linear current–voltage behaviour were obtained by fabricating ITO/GTO bilayer thin films with a Ga content of 25 mol%. Heat treatment at 200 °C is thought to be effective in producing the rectifying characteristics of the ITO/GTO bilayer thin films to the extent that the heat treatment does not crystallize the GTO thin films deposited at room temperature.

5.2 Recommendations for future work

Even though the objectives of this research are achieved, the research was carried out within the author's time constraints, and therefore, there are some avenues for further research. The recommendations for future work are given as follows:

1. To fabricate a thin film transistor based on GTO semiconductor.
2. To determine the I–V characteristics of the fabricated GTO-based thin film transistor.

REFERENCES

[1] K. Nomura, H. Ohta, K. Ueda, T. Kamiya, M. Hirano, and H. Hosono, "Thin-film transistor fabricated in single-crystalline transparent oxide semiconductor," *Science (80-.).*, vol. 300, no. 5623, pp. 1269–1272, 2003, doi: 10.1126/science.1083212.

[2] X. Z. Wang *et al.*, "Deposition of IGZO or ITZO thin films by co-sputtering of IZO and GZO or ITO targets," *Adv. Mater. Res.*, vol. 1110, pp. 197–202, 2015, doi: 10.4028/www.scientific.net/amr.1110.197.

[3] T. Matsuda, K. Umeda, Y. Kato, D. Nishimoto, M. Furuta, and M. Kimura, "Rare-metal-free high-performance Ga-Sn-O thin film transistor," *Sci. Rep.*, vol. 7, pp. 44326(1–7), 2017, doi: 10.1038/srep44326.

[4] M. Grundmann, *The Physics of Semiconductors: An Introduction Including Nanophysics and Applications Third Edition*. Springer, 2016.

[5] K. Blankenbach, A. Hudak, and M. Jentsch, "Direct drive, multiplex and passive matrix," in *Handbook of Visual Display Technology*, 2012, pp. 417–437.

[6] H. Frenzel, A. Lajn, and M. Grundmann, "One decade of fully transparent oxide thin-film transistors: Fabrication, performance and stability," *Phys. Status Solidi - Rapid Res. Lett.*, vol. 7, no. 9, pp. 605–615, 2013, doi: 10.1002/pssr.201307259.

[7] J. S. Park, W. J. Maeng, H. S. Kim, and J. S. Park, "Review of recent developments in amorphous oxide semiconductor thin-film transistor devices," *Thin Solid Films*, vol. 520, no. 6, pp. 1679–1693, 2012, doi: 10.1016/j.tsf.2011.07.018.

[8] E. Fortunato, P. Barquinha, and R. Martins, "Oxide semiconductor thin-film transistors: A review of recent advances," *Adv. Mater.*, vol. 24, no. 22, pp. 2945–2986, 2012, doi: 10.1002/adma.201103228.

[9] Y. Kuo, "Thin film transistor technology - Past, present, and future," *The Electrochemical Society Interface*, vol. 22, no. 1, pp. 55–61, 2013.

[10] M. Rose, "Active Matrix Liquid Crystal Displays (AMLCDs)," in *Handbook of Visual Display Technology*, 2012, pp. 1590–1606.

[11] M. Grundmann, H. Frenzel, A. Lajn, M. Lorenz, F. Schein, and H. Von Wenckstern, "Transparent semiconducting oxides: Materials and devices," *Phys. Status Solidi Appl. Mater. Sci.*, vol. 207, no. 6, pp. 1437–1449, 2010, doi: 10.1002/pssa.200983771.

[12] A. P. P. Correia, C. Barquinha, P. M. Goes, and J. C. da Palma, "Chapter 2: Thin-Film Transistors," in *A Second-Order ΣΔ ADC Using Sputtered IGZO TFTs*, Springer, 2016, pp. 5–15.

[13] P. Barquinha, R. Martins, L. Pereira, and E. Fortunato, "Chapter 5: The (R)evolution of Thin-Film Transistors (TFTs)," in *Transparent Oxide Electronics: From Materials to Devices*, 2012, pp. 155–209.

[14] H.-H. Hsieh, H.-H. Lu, H.-C. Ting, C.-S. Chuang, C.-Y. Chen, and Y. Lin, "Development of IGZO TFTs and their applications to next-generation flat-panel displays," *J. Inf. Disp.*, vol. 11, no. 4, pp. 160–164, 2010, doi: 10.1080/15980316.2010.9665845.

[15] K. Nomura, H. Ohta, A. Takagi, T. Kamiya, M. Hirano, and H. Hosono, "Room-temperature fabrication of transparent flexible thin-film transistors using amorphous oxide semiconductors," *Nature*, vol. 432, no. 7016, pp. 488–492, 2004, doi: 10.1038/nature03090.

[16] "新しい結晶性酸化物半導体CAAC (C-Axis Aligned Crystal)," *Semiconductor Energy Laboratory Co., Ltd.*, 2012. https://www.sel.co.jp/images/news/igzo/caac.pdf (accessed Nov. 29, 2018).

[17] A. Feltrin and A. Freundlich, "Material considerations for terawatt level deployment of photovoltaics," *Renew. Energy*, vol. 33, pp. 180–185, 2008, doi: 10.1016/j.renene.2007.05.024.

[18] U. S. G. Survey, "Mineral Commodity Summaries 2018," 2018. [Online]. Available: https://minerals.usgs.gov/minerals/pubs/mcs/2018/mcs2018.pdf.

[19] H. Fukushima, M. Yuge, T. Matsuda, and M. Kimura, "Evaluation of Ga-Sn-O Films fabricated using Mist Chemical Vapor Deposition," in *2016 IEEE International Meeting for Future of Electron Devices, Kansai (IMFEDK)*, 2016, pp. 1–2.

[20] R. Okamoto, H. Fukushima, M. Kimura, and T. Matsuda, "Characteristic evaluation of Ga-Sn-O films deposited using mist chemical vapor deposition," in *2017 IEEE International Meeting for Future of Electron Devices, Kansai (IMFEDK)*, 2017, pp. 74–75, doi: 10.1109/IMFEDK.2017.7998049.

[21] Y. Kato, K. Umeda, D. Nishimoto, T. Matsuda, and M. Kimura, "Characteristic evaluation of Ga-Sn-O thin films fabricated using RF magnetron sputtering," in *2016 IEEE International Meeting for Future of Electron Devices, Kansai (IMFEDK)*, 2016, pp. 1–2, doi: 10.1109/IMFEDK.2016.7521680.

[22] R. Takagi, K. Umeda, M. Kimura, and T. Matsuda, "Room-temperature forming of Ga-Sn-O film for thin-film transistors," in *2017 IEEE International Meeting for Future of Electron Devices, Kansai (IMFEDK)*, 2017, pp. 68–69, doi: 10.1109/IMFEDK.2017.7998046.

[23] T. Matsuda, R. Takagi, K. Umeda, and M. Kimura, "Room-temperature fabrication of a Ga-Sn-O thin-film transistor," *Solid. State. Electron.*, vol. 134, pp. 19–21, 2017, doi: 10.1016/j.sse.2017.05.006.

[24] H. P. Dang, Q. H. Luc, V. H. Le, and T. Le, "The influence of deposition temperature and annealing temperature on Ga-doped SnO2 films prepared by direct current magnetron sputtering," *J. Alloys Compd.*, vol. 687, pp. 1012–1020, 2016, doi: 10.1016/j.jallcom.2016.06.236.

[25] S. Swann, "Magnetron sputtering," *Phys. Technol.*, vol. 19, no. 2, pp. 67–75, 1988, doi: 10.1088/0305-4624/19/2/304.

[26] S. Nie, A. Liu, Y. Meng, B. Shin, G. Liu, and F. Shan, "Solution-processed ternary p-type CuCrO2 semiconductor thin films and their application in transistors," *J. Mater. Chem. C*, vol. 6, no. 6, pp. 1393–1398, 2018, doi: 10.1039/c7tc04810f.

[27] BYJU'S, "junction field-effect transistor (JFET)," *https://byjus.com/physics/junction-field-effect-transistor/*, 2023. https://byjus.com/physics/junction-field-effect-transistor/ (accessed Jul. 07, 2023).

[28] Fahad, "pn junction and semiconductor diodes," *https://www.electroniclinic.com/pn-junction-in-semiconductor-diodes/*, 2022. https://www.electroniclinic.com/pn-junction-in-semiconductor-diodes/ (accessed Jul. 07, 2023).

[29] T. Moriga, T. Okamoto, K. Hiruta, A. Fujiwara, I. Nakabayashi, and K. Tominaga, "Structures and physical properties of films deposited by simultaneous DC sputtering of ZnO and In2O3 or ITO targets," *J. Solid State Chem.*, vol. 155, no. 2, pp. 312–319, 2000, doi: 10.1006/jssc.2000.8919.

[30] K. Tominaga *et al.*, "Conductive transparent films deposited by simultaneous sputtering of zinc-oxide and indium-oxide targets," *Vacuum*, vol. 59, no. 2–3, pp. 546–552, 2000, doi: 10.1016/S0042-207X(00)00314-6.

[31] T. Moriga *et al.*, "Transparent conducting amorphous Zn–Sn–O films deposited by simultaneous dc sputtering," *J. Vac. Sci. Technol. A*, vol. 22, no. 4, pp. 1705–1710, 2004, doi: 10.1116/1.1765658.

[32] T. Moriga *et al.*, "In2O3-ZnO transparent conductive oxide film deposition on polycarbonate substrates," *Vacuum*, vol. 83, no. 3, pp. 557–560, 2009, doi: 10.1016/j.vacuum.2008.04.051.

[33] 石橋和也, "β -Ga2O3薄膜へのSn ドーピング効果," pp. 4–5.